

UNIVERSITÀ DEGLI STUDI DI MILANO

Facoltà di Scienze e Tecnologie Laurea Triennale in Fisica

Probing the Static Depinning Transition of a Crystal-Quasicrystal Interface

Advisor: Prof. Nicola Manini

Co-advisor: Dr. Andrea Vanossi

Davide Gay Matricola n° 971842 A.A. 2023/2024

Probing the Static Depinning Transition of a Crystal-Quasicrystal Interface

Davide Gay

Dipartimento di Fisica, Università degli Studi di Milano, Via Celoria 16, 20133 Milano, Italia

21 February, 2025

Abstract

We study a model consisting of a crystalline monolayer with hexagonal symmetry in contact with a decagonal quasicrystalline potential, at the optimal angular orientation according to the extension of the Novaco-McTague theory to the case of a quasicrystalline potential. Through FIRE minimization and Simulated Annealing, we obtain a well-relaxed configuration of the monolayer, which is used as the starting configuration for the friction analysis. The frictional properties of the monolayer are then studied using molecular dynamics simulations, exploring the Aubry-type transition between a superlubric state and one characterized by a finite static friction force.

Advisor: Prof. Nicola Manini Co-Advisor: Dr. Andrea Vanossi

Contents

1	Inti	roduction	3
	1.1	The Frenkel-Kontorova model	3
	1.2	The Novaco-McTague theory	4
2	The	e model	6
3	Imp	blementation	7
	3.1	Static relaxation	8
	3.2	FIRE minimization	9
	3.3	Simulated Annealing	10
	3.4	Friction protocol	13
	3.5	Steady states	14
4	Res	ults	16
	4.1	Static properties	16
	4.2	Frictional properties	17
	4.3	Depinning transition	20
5	Dis	cussion and Conclusion	21

1 Introduction

1.1 The Frenkel-Kontorova model

The frictional properties at the contact of two periodic interfaces have long attracted interest in research, and various models have been developed for the study of these systems. The Frenkel-Kontorova (FK) model is the simplest model used to described a 1D chain of interacting particles on a periodic potential substrate [1, 2]. The simplest formulation of FK model consists in a chain of particles in a sinusoidal potential, interacting harmonically with their first neighbours. The Hamiltonian for this model is:

$$H = \sum_{i}^{N} \left[\frac{p_i}{2m} + \frac{K}{2} (x_{i+1} - x_i - a_{coll})^2 + \frac{U_0}{2} \left(1 - \cos \left(\frac{2\pi}{a_{pot}} x_i \right) \right) \right], \tag{1}$$

where a_{coll} is the rest distance of the harmonic interaction and a_{pot} is the potential spacing. From here we can define a mismatch ratio $\rho = \frac{a_{pot}}{a_{coll}}$ between the number of particles and the potential wells. The case $\rho = 1$ describes a lattice-matched system, with one particle in each well.

A kink or soliton is the topological excitation caused by an addition of a particle to this chain. The presence of an additional particle would result in two particles being placed inside the same potential well. Once the particle is added to the chain, it pushes out of their wells few surrounding particles and the equilibrium configuration is characterized by a local compression of the chain - a kink; on the other hand, the subtraction of a particle leaves a well empty and the equilibrium configuration is characterized by a local expansion of the chain, called antikink. Kinks and antikinks push particles out of the minima of the substrate potential, allowing them to move easily in response to an external driving force. As the FK model can be solved exactly in the continuum approximation, it has been long adopted as the standard model in describing soliton excitation.

A particular case of interest is given by that in which the ratio ρ is an irrational number, known as an incommensurate case. In the incommensurate case, the FK model shows an interesting transition as a function of the potential height V_0 . Below a well defined value of V_0 the chain can slide freely over the substrate under the action of an arbitrarily small driving force, i.e. the static friction F_s vanishes. This condition is called superlubricity. In contrast, above the critical value, the system shows a finite F_s which must be overcome to start sliding. This transition, defined as transition by breaking of analyticity, was studied in great detail by Serge Aubry [3, 4], and it is therefore widely known as

the Aubry transition. The parameter

$$g = \frac{V_0}{ka_{coll}^2} \tag{2}$$

represents the relative amplitude of the corrugation potential respect to the natural energy unit of the colloid lattice. If $g \gg 1$, more particles are located near the bottom of potential wells, therefore requiring a very large force to force them out of the potential barrier and move the chain globally. On the contrary, if $g \ll 1$, particles composing the chain can be easily dragged by weaker forces, producing a sliding motion.

1.2 The Novaco-McTague theory

We consider a 2D harmonic crystalline monolayer, having the following Hamiltonian

$$H_0 = \sum_{j} \frac{\mathbf{p}^2}{2M} + \frac{1}{2} \sum_{j,j'} \phi_{j,j'}^{\alpha \alpha'} \mathbf{u}_{j,\alpha} \mathbf{u}_{j',\alpha}$$
(3)

where $\mathbf{u}_j = \mathbf{r}_j - \mathbf{R}_j$ is the displacement from the equilibrium lattice positions \mathbf{r}_j of the *j*-th particle, and ϕ is the Hessian matrix of the interaction potential. The quasiperiodic substrate corrugation is modeled as a local potential

$$V(\mathbf{r}) = -V_0 \left| \sum_{j=1}^{N_s} \frac{e^{i\mathbf{k}_j \cdot \mathbf{r}}}{N_s} \right|^2 = -\frac{V_0}{N_s^2} \left(\sum_G e^{-i\mathbf{G} \cdot \mathbf{r}} + N_s \right)$$
(4)

where V_0 is the corrugation potential amplitude, a_{pot} is the characteristic length scale of the potential and the integer N_s denotes the N_s -fold symmetry of the potential. \mathbf{k} are the reciprocal vectors generating the potential:

$$\mathbf{k}_{m} = \frac{2\pi}{a_{pot}} \left(\cos \frac{2\pi (m-1)}{N_{s}}, \sin \frac{2\pi (m-1)}{N_{s}} \right)$$
 (5)

and G are the vectors connecting the $N_s(N_s-1)$ pairs of **k**:

$$G = \mathbf{k}_m - \mathbf{k}_n, \quad m \neq n \tag{6}$$

Fig. 1 shows the set of G vectors for a 5-fold symmetry. Their modules can be calculated with some trigonometry:

$$|\mathbf{G_1}| = \frac{2\pi}{a_{pot}} \sqrt{\frac{2\sqrt{5}}{1+\sqrt{5}}} \quad \text{and} \quad |\mathbf{G_2}| = \frac{2\pi}{a_{pot}} \sqrt{\frac{5+\sqrt{5}}{2}}$$
 (7)

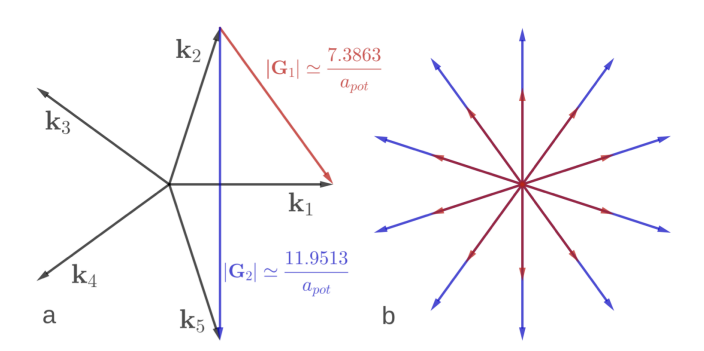


Figure 1: (a) \mathbf{G} vectors and their geometric construction from the 5 \mathbf{k} vectors of the 5-fold potential. (b) The complete set of 20 \mathbf{G} vectors.

For simplicity, we remove the constant additive term in Eq. 4 to obtain a zero average potential:

$$V(\mathbf{r}) = -\frac{V_0}{N_s^2} \sum_G e^{-i\mathbf{G}\cdot\mathbf{r}}$$
(8)

The global Hamiltonian is therefore

$$H = H_0 + U_{ext} = H_0 + \sum_{i} V(\mathbf{r_j})$$
(9)

Following Novaco and McTague [5, 6], we apply the one-phonon approximation: for small displacements, we can expand the exponential as $e^{-i\mathbf{G}\cdot\mathbf{u}} \approx 1 - i\mathbf{G}\cdot\mathbf{u}$. The first part of this work is dedicated to performing static optimizations, i.e. we search for a configuration that minimizes the potential energy. In this context, the Novaco-McTague theory predicts in the limit $V_0 \to 0$, using a variational approach:

$$\begin{cases} \epsilon_{1-ph} = -\frac{V_0^2}{2MN_s^4} \sum_{\mathbf{q}}^{BZ/O} \sum_{s=L,T} \frac{|f_{\mathbf{q},s}|^2}{\omega_{\mathbf{q},s}^2} \\ f_{\mathbf{q},s} = \sum_{\mathbf{G}} \sum_{\tau} \mathbf{G} \cdot \epsilon_{\mathbf{q},s} e^{-i\tau \cdot \mathbf{R}_0} \delta_{\mathbf{q},\mathbf{G}-\tau} \end{cases}$$

Here R_0 is the origin of the lattice, τ are the crystal reciprocal lattice vectors, $\omega_{\mathbf{q},s}$ and $\epsilon_{\mathbf{q},s}$ are the phonon frequencies and phonon polarization vectors, while s = L, T indicates the phonon branch (longitudinal or transverse).

Through the integer N_s , the Novaco-McTague theory can naturally be applied to both the crystalline case ($N_s = 3$) and the quasicrystalline case, selecting $N_s = 5$ as done in this work. While the crystalline case has long been the object of several studies, the quasicrystalline case has hardly been explored until recently.

In the crystalline case, it is known that there exists a privileged orientational epitaxy between the colloidal lattice and the substrate potential. The existence of a nonzero optimal misfit angle emerges from NM theory and has subsequently

been verified experimentally [7, 8]. Studies conducted in recent years showed that this result can be extended to the quasicrystalline case [9, 10, 11, 12].

Most recently, Ref. [13] has provided analytical predictions for the optimal misfit angle which are shown to be in perfect agreement with numerical optimization. In the first part of this work we reproduce the relaxation energetics of a model hexagonal crystal over a quasiperiodic potential substrate at the optimal misfit angle and verify that our results are in agreement with those of Ref. [13]. In the second part, we aim to investigate the tribological properties of the model under the action of a constant external driving force, looking for evidence of an Aubry-type transition from a superlubric to a pinned configuration.

2 The model

The model adopted in our work consists of a 2D colloidal monolayer interacting with a decagonal quasi-periodic substrate in a viscous fluid. The use of colloids in place of atoms has long introduced in this field of study in order for the particles to be visible under a microscope, allowing direct experimental observations. This model is described by the Hamiltonian:

$$H_{tot} = \sum_{i} \frac{\mathbf{p}^2}{2M} + U_{cc} + U_{ext} + U_F \tag{10}$$

Here U_{cc} indicates the intercolloidal potential, U_{ext} is the potential resulting from the presence of the quasicrystalline substrate as described by the Novaco-McTague theory presented in the previous section, and U_F is the potential associated with the external driving force applied in dynamical simulations. The intercolloidal potential adopted in this work is a simple harmonic potential:

$$U_{cc} = \frac{K}{2} \sum_{i,j} (|\mathbf{r}_i - \mathbf{r}_j| - a_{coll})^2$$
(11)

where K is the spring constant. Anharmonic potentials such as the Yukawa potential or screened Coulomb potential would describe the interactions at play more realistically and have been used in previous studies. However, the choice of a harmonic interaction allows for better comparisons with the Novaco-McTague theory.

The resulting equation of motion for the j-th colloidal particle is:

$$m\ddot{\mathbf{r}}_{j}(t) = -m\gamma\dot{\mathbf{r}}_{j}(t) - \nabla_{\mathbf{r}_{n}}(U_{cc} + U_{ext}) + F\hat{\mathbf{x}}$$
(12)

where $-m\gamma\dot{\mathbf{r}}_{j}(t)$ is a term associated with the damped motion of the particle inside a viscous fluid and F is the external driving force that, for definiteness,

Parameter	Value
m	31.06 fkg
γ^{-1}	$5 \cdot 10^3 \text{ µs}$
K	$0.2 \text{ zJ} \text{µm}^{-2}$
a_{pot}	$5.4~\mu\mathrm{m}$
a_{coll}	5.8 μm
Ka_{coll}^2	$6.728 \mathrm{\ zJ}$

Table 1: Parameters used in our model. The value a_{pot} will be used as natural unit for the distance, while Ka_{coll}^2 is used as natural unit for energy, with $g = \frac{V_0}{Ka_{coll}^2}$ being the dimensionless parameter used to express the corrugation potential amplitude.

we apply in the direction of the \hat{x} axis, which is a high-symmetry axis of the quasicrystalline potential. The temperature of the system is assumed to be zero.

We observe that due to the decagonal symmetry of the potential and to the symmetries of the triangular lattice, the problem repeats periodically every $0^{\circ}-12^{\circ}$ of mutual rotation. Furthermore, the angular inversion symmetry $\theta \to -\theta$ in the potential can reduce the nontrivial range to $0^{\circ}-6^{\circ}$.

Table 1 reports the parameters adopted in this model, from which we can define the natural energy scale as $ka_{coll}^2 = 6.728 \,\mathrm{zJ}$. The dimensionless parameter describing the corrugation potential amplitude will then be $g = \frac{V_0}{ka_{coll}^2}$, in analogy with the FK model parameter introduced in Eq. (2).

3 Implementation

In this section we present the technical implementation of the physical model as described in Sect. 2. In order to perform relaxations and dynamical simulations, we will use LAMMPS (Large-scale Atomic/Molecular Massively Parallel Simulator), a classical Molecular Dynamics (MD) software [14].

Firstly, we generate a circular sample from a hexagonal lattice with spacing a_{coll} . The sample consists of N colloids. The generated lattice sample will be placed in the center of a 2D simulation supercell approximately 10 times larger than the sample itself, large enough to accommodate the full time evolution in all simulations we are running. We apply periodic boundary conditions at the edges of the cell to prevent nonphysical bouncing of the particles on a box edge. Fig. 2 shows an example of a relatively small hexagonal lattice of N = 3463 particles

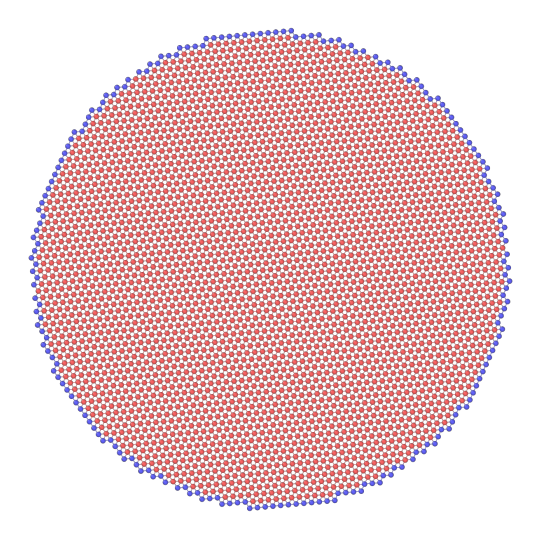


Figure 2: A visual rendering of a relatively small colloid lattice sample as used in this work, made of N=3463 particles rotated by $\theta_{NM}\simeq 5.305^{\circ}$. Blue particles $(N_{ext}=204)$ are considered the 'frame' of the sample. In the initial relaxation they are locked in their lattice positions, while the red 'internal' particles $(N_{int}=3259)$ are free to move under the action of the substrate potential and their reciprocal interactions. In subsequent sliding simulations, the blue particles are treated as a rigid body.

rotated at the Novaco angle.

3.1 Static relaxation

For each value of interest of $g = V_0/ka_{coll}^2$, we need a static configuration that minimizes the potential energy of the system before performing friction simulations. All simulations in this work are performed with the sample lattice rotated, with respect to the substrate potential, by the Novaco-McTague angle i.e. the angle that minimizes the potential energy. For the adopted configuration of $a_{pot} = 5.4 \, \mu m$, $a_{coll} = 5.8 \, \mu m$, the optimal misfit angle is $\theta_{NM} \simeq 5.305^{\circ}$ [13].

A first necessary step for setting up the simulation runs consists in establishing the appropriate MD integration time step δt . Ideally, the appropriate time step is large enough to respect total energy conservation over a time interval compatible with that required by our simulations, while also being small enough to not cause the computation time to increase unnecessarily. This is achieved by performing MD simulations in which the particles are only subject to the potential $U = U_{cc} + U_{ext}$, not to any external constant driving force nor to any

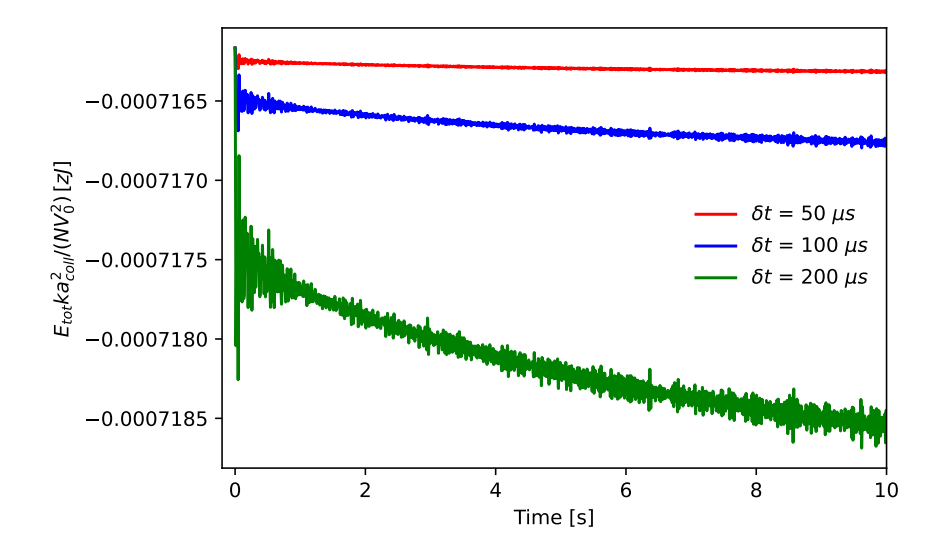


Figure 3: A verification of the conservation of the total energy over conservative simulations, for a sample lattice of N=9407, all started off at the same initial condition. The corrugation potential amplitude is g=0.1. Note the significant jump in the total energy at the first time step, a characteristic defect of the Velocity Verlet algorithm when started off with all null velocities. Smaller time steps produce better energy conservation.

nonconservative damping. Fig. 3 shows the supposedly conserved total energy E_{tot} as function of the simulation time, for a few selected time step δt . As we can observe, the value $\delta t = 50\,\mu s$ keeps the total energy quite constant over the relatively long simulated time, and is therefore the chosen integration time step for our MD simulations. Note that atomic MD simulations usually require far smaller time steps, typically in the order of one fs, and this makes the 50 micro s time step appropriate. However, we are dealing with colloids which are far heavier and therefore slower.

For relaxation, a number of numerical methods can be implemented. The next two subsections summarize the methods adopted in this work and their implementation.

3.2 FIRE minimization

In the weak-coupling region, where $g \ll 1$, we expect displacements of the atoms proportional to V_0 and a lowering in the total energy of the system proportional to V_0^2 (Eq. 1.2). This weak-coupling perturbative regime is compatible

with a single global minimum at a configuration very close to the perfect crystal.

FIRE, short for Fast Inertial Relaxation Engine, is a computational relaxation method used to quickly find the nearest local minimum from the starting configuration, as described in detail in Ref. [15]. It is based on the discrete version of the following equation:

$$\dot{\mathbf{v}}(t) = \frac{\mathbf{F}}{m} - \gamma(t)|\dot{\mathbf{v}}(t)| \left(\frac{\mathbf{v}(t)}{|\mathbf{v}(t)|} - \frac{\mathbf{F}(t)}{|\mathbf{F}(t)|} \right)$$
(13)

where m and \mathbf{v} are the mass and the velocity of a particle, and $\mathbf{F} = -\nabla U(\mathbf{x})$ is the force acting on it obtained from the potential $U = U_{cc} + U_{ext}$. The last term of Eq. (13) is an addition to the standard equation of damped motion whose purpose is to introduce an acceleration in a direction which is steeper than the current direction of motion, via $\gamma(t)$, when the power $P(t) = \mathbf{F}(t) \cdot \mathbf{v}(t)$ is positive. To avoid uphill motion, the velocity is set to zero if the power becomes negative. Furthermore, the velocity is also modified with:

$$\mathbf{v} = (1 - \alpha)\mathbf{v} + \alpha\mathbf{v} \frac{\mathbf{F}}{|\mathbf{F}|}$$
 (14)

using the parameter $\alpha = \gamma \delta t$, with δt being the integration time step. For our minimization runs, we use LAMMPS' default values for the most of the parameters involved. The only parameter worth tuning is the integration time step δt . According to Ref. [15], for atomic-scale molecular dynamics an estimate of correct time step is $\delta t = 10\delta t_{MD}$, where δt_{MD} is the integration time step used with regular MD simulations. Following this rule, we use $\delta t = 500\,\mu s$. Larger time steps would result in fluctuations around the energy minimum, failing to settle in the minimum in a satisfactory way - that is, reaching the energy or force thresholds required for the algorithm to stop.

The FIRE algorithm needs to be given a stopping condition either on the force acting upon the system or the energy lowering. After testing a few different conditions, we decide to set a threshold on the force only, requiring its value to reach that of $10^{-4}V_0/a_{coll}$ for the minimization run to stop.

3.3 Simulated Annealing

As the corrugation potential amplitude is increased, the potential becomes more and more rugged, as sketched in Fig. 4, presenting several local minima instead of a singular global minimum. Applying FIRE to this situation would only find the closest local minimum, while the global minimum could sit far away from the the current basin of attraction.

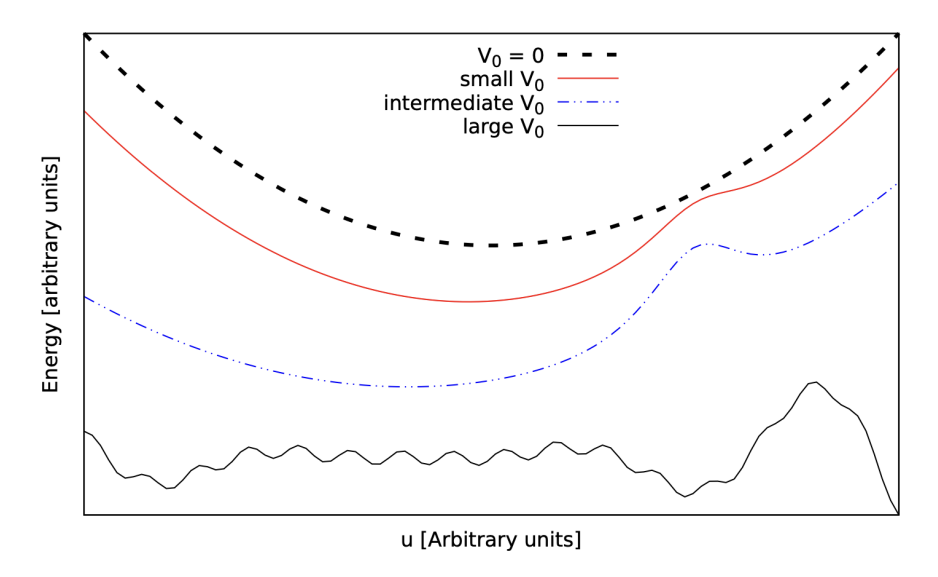


Figure 4: A 1D sketch of the total potential as a function of an arbitrary displacement coordinate. When the corrugation contribution remains within the perturbative range one global minimum is observed. As the corrugation amplitude is further increased, the potential becomes more and more rugged, presenting several local minima.

Simulated Annealing is a probabilistic computational method used to find a global minimum in the presence of several local minima. Its name comes from annealing, a technique used in metallurgy that involves heating and subsequently "slowly" cooling a material in order to alter its physical properties. The system is initially brought to an initial temperature T_0 . This temperature should be high enough to let the system explore configurations that sit outside the basin of attraction of a local minimum of the potential energy. For this reason a reasonable choice of initial temperature for our model involves a value of $k_B T_0$ comparable with the largest potential barrier. However, a value too high may lead to completely disordered configurations of the lattice sample. The choice of T_0 is therefore to be made with caution. As the maximum potential barrier in the model is determined by the value of V_0 , we start each annealing process from a temperature T_0 such that $k_B T_0 = 0.1 V_0$.

After bringing the system to the designed initial temperature, the system is cooled down following an annealing schedule. An annealing schedule establishes how the temperature is brought down in steps to T=0. Several different options can be adopted as to how the temperature is decreased, most notably:

• linearly;

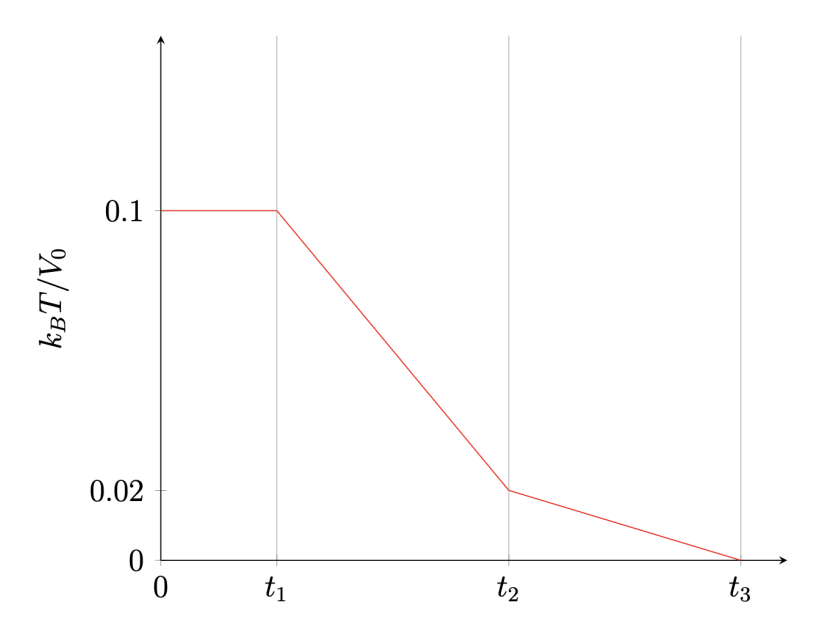


Figure 5: The adopted Simulated Annealing schedule.

• "geometrically", i.e. multiplying T by a factor $0 < \alpha < 1$, close to 1, at each step;

and with various other more elaborate or composite algorithms.

Simulated Annealing does not ensure that the global minimum is found over a finite simulation time. However, by choosing an effective annealing schedule and allowing the system enough time to be slowly cooled down, we can identify the resulting minimum as the global minimum with a good degree of confidence. For this work we chose to cool the system using series of linear ramps with different slopes, using LAMMPS Langevin thermostat. The adopted annealing schedule is depicted in Fig. 5. Equilibration times t_1, t_2, t_3 can be tuned as needed, however values $t_1 = 2.5 \, \text{s}, t_2 = 7.5 \, \text{s}, t_3 = 12.5 \, \text{s}$ were able to yield satisfactory results. Performing longer simulations or adding more linear ramps was not found to be helpful in locating final configurations characterized by a lower potential energy. At the end of the annealing, a FIRE minimization is performed to ensure that the precise minimum is reached.

In order to avoid global deformations of the sample during simulations, we decide to lock the external colloids of the sample in their lattice positions as a rigid frame, following previous studies [12]. In practice, in static minimizations the external particles are not allowed to move from their initial positions, by setting the total force acting on them as zero. In friction simulations, the outer ring particles are kept as a rigid body, allowed to translate freely under the action of the resulting total force.

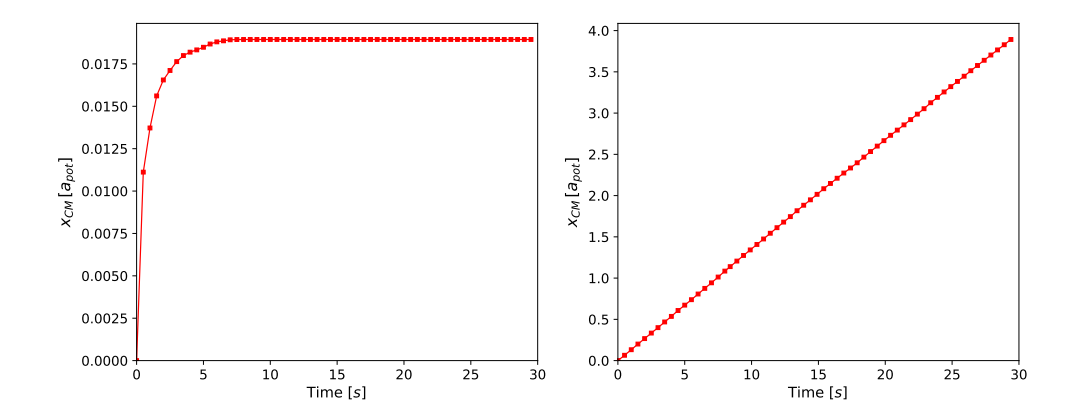


Figure 6: (a) Pinned state observed for g = 0.07, F = 0.01. (b) Unpinned state observed for g = 0.07, F = 0.05. In panel (a) we can observe clearly the presence of a transient before

reaching the pinned steady state.

3.4 Friction protocol

To study the frictional properties of the system, we start from perfect lattice configurations rotated by the optimal twist angle $\theta_{NM} \simeq 5.305^{\circ}$ and subsequently fully relaxed simulation. We then apply a constant dragging force F to the colloid directed along the x-axis.

Different values of g involve different scales for the forces and the resulting velocities involved in the study of the dynamical properties of the system. For each g we define the force F_{1s} , which is the minimum force needed by a single colloid to exit the potential well at the origin. The value of F_{1s} is given by:

$$F_{1s} = z \frac{V_0}{a_{pot}} \tag{15}$$

where $z = 4.279396 \pm 0.000001$. This is obtained by numerically computing the second derivative of the external potential $V(\mathbf{r})$ evaluated at the first inflection point [9]. It will therefore be natural as well as convenient to express forces in units of F_{1s} .

For every force applied, we aim to distinguish between a pinned state and an unpinned state. A pinned configuration is such that, after a transient, the center of mass velocity of the sample vanishes, see Fig. 6a. An unpinned configuration is such that the center of mass velocity of the sample fluctuates around a constant finite average value (Fig. 6b), resulting in approximately uniform linear motion of the sample.

We start by applying a range of forces separated by relatively large intervals, e.g. $0.1F_{1s}$. This allows us to roughly identify an interval of forces in which a

depinning transition may take place. For relatively large values of $g, g \ge 0.05$ or greater, we expect to find a transition between a pinned state and an unpinned one already between two of these forces. For smaller g, however, $F = 0.1F_{1s}$ is a force too great to observe pinned states. Once the interval in which the transition takes place has been determined, we proceed by probing more accurately the values within that interval, e.g. by increasing the force by $0.01F_{1s}$. We also similarly probe the interval immediately greater than the one containing the transition. This will be useful when trying to estimate the value of the static friction force F_s , as later described in detail in Sect. 4. In the case of large enough corrugation potential amplitudes this procedure may allow us to observe a pinned state at weak forces and therefore identify an interval for the transition, but not in all cases. With especially small g, a pinned state will not be observed: we may be in the presence of a superlubric configuration, that is one in which every force applied to the system, however weak, will cause the sample to slide in a linear motion. Ruling out the presence of a pinned state at lower forces than those studied is not achievable computationally: for any force that yields a running state, we cannot rule out that applying an even smaller force will result in a pinned state. Studying the frictional properties of the system therefore becomes increasingly difficult as the forces at play get smaller, since longer and longer simulation times are required for the sample to travel significant distances (i.e. at least a few times the potential characteristic length $a_{pot} = 5.4 \,\mu\text{s}$). In these cases we can only estabilish an upper boundary for the depinning force. Furthermore, as highlighted by Ref. [13] (and shown in Fig. 7), boundary effects are responsible for oscillations of the relaxed potential energy as the sample travels along the x axis. These oscillations act as potential barriers, thus ensuring that, for a small enough force, a pinned state will always be observed as long as the size is finite. To address this issue, the depinning transition should be investigated as a function of the sample size. Due to time constraint we were not able to carry out this task in full.

3.5 Steady states

To properly compute the frictional steady-state properties of the system, we must first of all identify a steady state, namely a state in which the velocity of the center of mass of the system does not change significantly over time, but rather fluctuates quickly around a constant mean value. For all cases of study, the system first undergoes a transient phase. The Langevin thermostat generating a damped dynamic keeps the temperature of the system close to T = 0. Its damping time constant, γ^{-1} , indicates the approximate time that it takes for the system

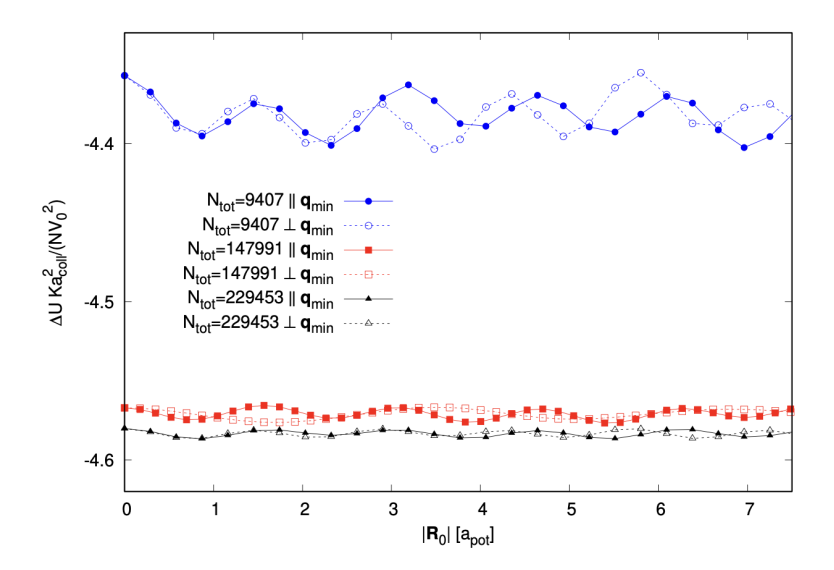


Figure 7: Effect of the translation \mathbf{R}_0 of the sample lattice center across the substrate potential for different sample sizes. With increasing size, the observed oscillations decrease in amplitude, suggesting that they would vanish in the infinite-size limit. Simulations carried out with values $a_{pot} = 5.4 \,\mu s$, $\theta = \theta_{NM}$, g = 0.0001 [13]. The direction $\perp \mathbf{q}_{min}$ are oblique directions at the Novaco angle.

to approach thermal equilibrium. In many situations, especially with forces far from depinning, a steady state is reached quickly, i.e. in times comparable to γ^{-1} . In many other cases, however, the system takes significantly longer times to reach a steady state, due to complex internal phenomena: during this transient phase the sample could incur in local depinning, while most of the sample remains locked, or full re-organization of the lattice particles, before eventually reaching a completely still configuration, or instead generate an avalanche-like depinning motion. For these reasons identifying a steady state can be a tricky task, more so because the total time duration of these transient phases can reach time intervals approaching 50 s, extending the computational time required for these simulations substantially.

Starting from a small force, we will run the simulation until a steady state is reached and long enough so that the sample center of mass is allowed to travel a distance greater than a few times a_{pot} . Starting from the resulting final state, we then increase the force by a small step and again reach and maintain a steady state. All transients are then discarded from the computation of the average center-mass velocity.

4 Results

4.1 Static properties

Firstly, we verify how our simulated regimes compare with the NM theory. In particular we compare our relaxed energies with the the results obtained by Ref. [13] regarding the deviation from analytical one-phonon prediction, Eq. (1.2), for increasing g. We study the relation between the relaxed energy at the optimal twist angle (NM angle) θ_{NM} for our choice of a_{pot}/a_{coll} and at different $g = V_0/ka_{coll}^2$.

For each value of interest of g ranging from 0.0001 to 1.0, we rotate the perfect lattice sample by the angle $\theta_{NM} \simeq 5.305$, perform complete optimization of the system and compute the energy lowering per internal particle $\Delta U/N_{int}$. Since the corrugation potential as defined in Eq. (8) is zero-average, we expect the potential energy per particle of an infinite hexagonal lattice sample to vanish. This is due to the incommensurability between the two geometries (hexagonal and decagonal), which results in every lattice particle being a random sampling of the zero-average potential. In the finite size case, the energy exhibits fluctuations around zero as function of the twist angle. The amplitude of these fluctuations is shown to decrease for increasing size faster than $N_{tot}^{-1/2}$ [13]. In order to counteract the effects of the sample edge, as was done in Ref. [13], we report the energy lowering $\Delta U = U_{relaxed} - U_{initial}$ instead of the absolute energy.

The results, shown in Fig. 8, are consistent with those of Ref .[13]. At low potential corrugation amplitudes, $g \leq 0.001$, where the weak-coupling approximation of the Novaco-McTague theory is valid, we observe that the energy lowering per particle is nearly constant, close to the value predicted by NM theory at the optimal misfit angle, whereas for greater values of g it deviates significantly.

Fig. 8 also allows us to compare the results obtained by a full relaxation run (Simulated Annealing to target the global potential energy minimum, plus FIRE to reach the bottom of the potential well) with those obtained by merely reaching the nearest local minimum with a single FIRE run. In the weak-coupling region the energy is proportional to V_0^2 as predicted by the NM theory (Eq. 1.2): in this region both methods are equally effective, as expected, at finding the global minimum. But as the corrugation amplitude is increased the rugged aspect of the potential makes Simulated Annealing essential for identifying the global energy minimum.

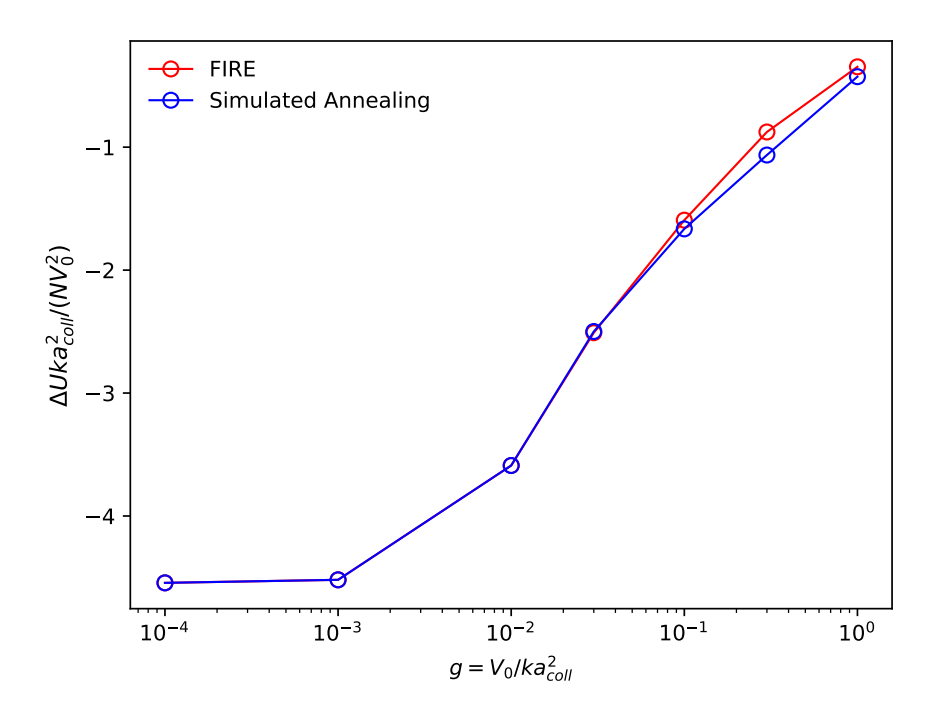


Figure 8: Relaxation energy per internal particle dependence on the corrugation amplitude for a circular sample of $N_{tot} = 81619$ particles. The energy per particle is computed accounting for the $N_{int} = 80527$ internal particles only. Results are compared between FIRE and complete Simulated Annealing optimization, as described in Sect. 3. For values up to g = 0.3, the two methods yield identical results. For larger g, Simulated Annealing is able to reach a deeper, possibly global, minimum.

4.2 Frictional properties

In order to study the frictional properties of the system, we apply a constant driving force F along the x axis to a lattice sample that has undergone a minimization run at the optimal twist angle θ_{NM} . As outlined in Sect. 3, measuring the steady-state velocity of a configuration requires reaching a steady state after going through a transient phase. Such transient phases can present varied aspects and can protract for long time intervals, making the identification of steady states a non trivial task. Fig. 9, shows a transient in the center-of-mass velocity of the sample encountered in our simulations.

Once a steady state has been reached, we measure the average velocity of the sample over a distance spanning at least a few times a_{pot} . The best possible

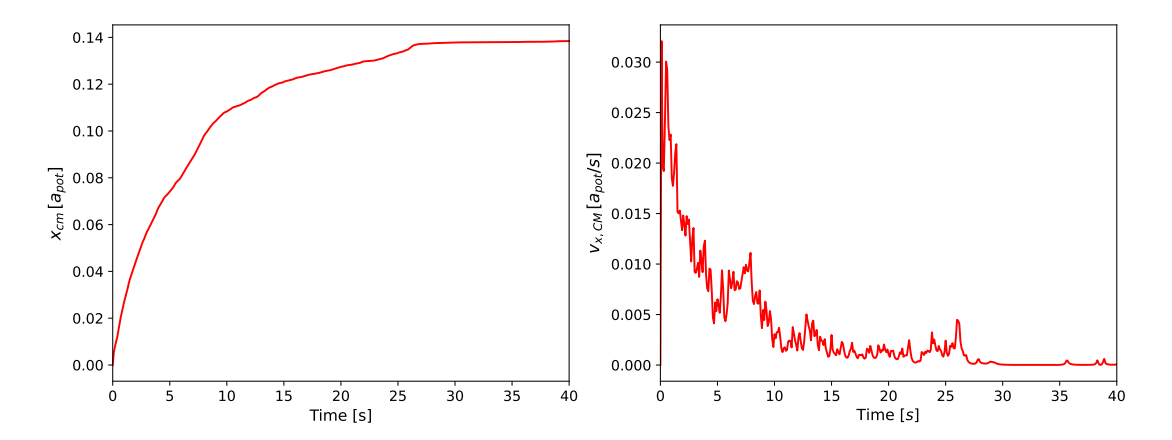


Figure 9: Center of mass displacement along the x axis (left) and center-of-mass velocity (right) as a function of the simulation time, for a lattice sample of N = 9407 particles, obtained imposing a normalized driving force $F = 0.04 F_{1s}$ over a substrate potential characterized by g = 0.08.

estimate is simply:

$$\langle v_{x,cm} \rangle = \frac{\Delta x_{cm}}{\Delta t} \tag{16}$$

where Δx_{cm} is the distance traveled along the x axis by the center of mass over a time Δt . An estimate of statistical uncertainty is provided by a standard deviation on the velocity of the particle in the steady state.

We then define the average mobility along the x axis as:

$$\mu_x = \frac{\langle v_{x,cm} \rangle}{F} \tag{17}$$

where F is the dragging force applied to the sample. In the simplest ideal case of a single free-sliding colloidal particle, the steady-state velocity is proportional to the driving force:

$$v_s = \frac{F}{m\gamma} \tag{18}$$

where γ is the damping rate. From this follows that the mobility of a single free-sliding particle is:

$$\mu_{free} = \frac{1}{m\gamma} \tag{19}$$

which is fixed by the simulation parameters. We call this quantity the free-sliding mobility.

We proceed to compute the steady-state mobility as function of the applied force. Fig. 10 shows the mobility along the x axis for a number of different g values. For higher g, we can observe clearly the presence of a transition from

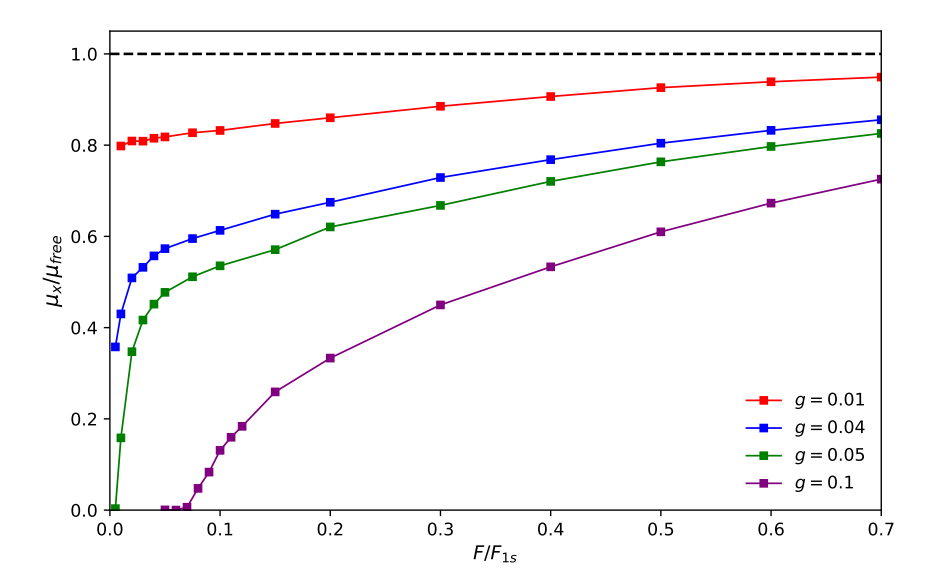


Figure 10: Normalized mobility μ_x/μ_{free} along the x axis as function of the driving force F/F_{1s} for different values of corrugation potential amplitude g, for a lattice sample of N=9407 particles. A depinning transition is clearly visible in some of the observed configurations.

pinned states, where the mobility is close to zero, to unpinned states with nonzero mobility. Low values of g, namely those lower than g=0.05, do not show evidence of pinned states in the range of forces measured. This absence of a static friction threshold could be indicative of a superlubric configuration even though, as outlined in Sect. 3, we cannot completely rule out the presence of pinned states at even weaker forces than those probed.

Additionally, we compute the steady-state velocity along the y axis in a similar fashion. We can thus measure the angle between the velocity and the applied force as:

$$\theta = \arctan\left(\frac{\langle v_{y,cm}\rangle}{\langle v_{x,cm}\rangle}\right). \tag{20}$$

By reporting the angle of steady-state motion as a function of the applied force we can check for evidence of directional-locking, that is a condition in which for a range of applied force F the sample slides at a fixed angle θ to the force. As shown in Fig. 11, for g = 0.07 we observe directional locking at low values of F at an angle $\theta \approx 28^{\circ}$.

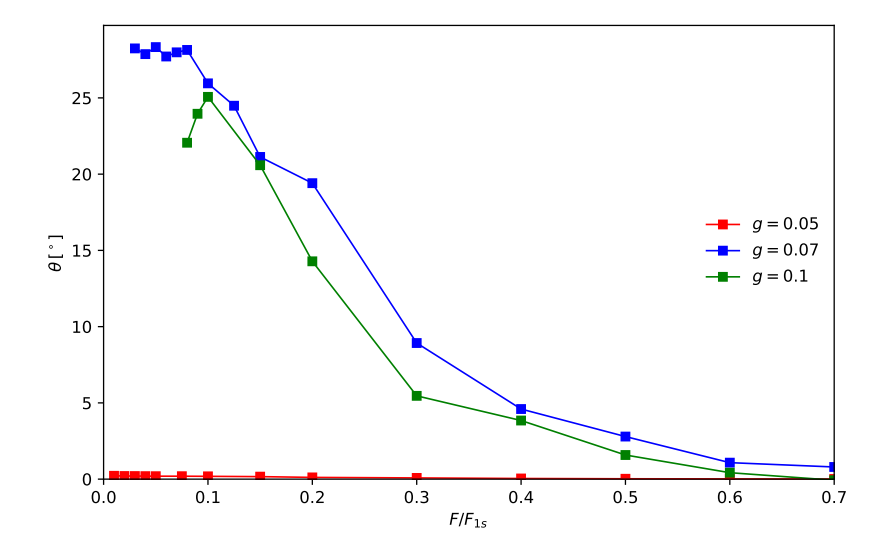


Figure 11: Angle θ between the velocity and the applied force as function of F/F_{1s} . The sample size is $N_{tot} = 9407$.

4.3 Depinning transition

To address the Aubry-type transition in the present model, for each value of g investigated we report a range of confidence for the static friction threshold. In order to achieve that, we take the largest force which leads to a clearly pinned steady state as a lower limit, and the weakest force which leads to a clearly unpinned configuration as an upper limit. When we fail to detect any statically pinned state, the lower limit is set to zero. Furthermore, in this window we estimate the static friction force F_s from the data. In-depth studies of a 1D crystal-on-crystal model have shown that in non-superlubric configurations μ approaches the pinning transition (with forces approaching the static friction threshold from above) with the shape of a power law with exponent $1/2 < \alpha < 1$ [2]. We attempt to identify the same power law for the crystal-on-quasicrystal case, Fig. 10. We then fit our mobility data with the following function:

$$\frac{\mu}{\mu_{free}} = B \left(\frac{F - F_s}{F_{1s}} \right)^{\alpha} . \tag{21}$$

The fitting parameters are B > 0, $F_s \ge 0$ and $0 < \alpha < 1$. This method provides a reliable estimate for F_s . We thus perform a fit with the function above using the measured mobility for a range of forces that extends from the first unpinned state to a force $0.1 F_{1s}$ greater. Using values beyond this range would be inappropriate, since the shape of the curve deviates from the power law, as shown in Fig. 12.

The resulting confidence ranges and estimated static friction thresholds are reported in Fig. 13 as functions of g. Fig. 13 places the Aubry transition in the

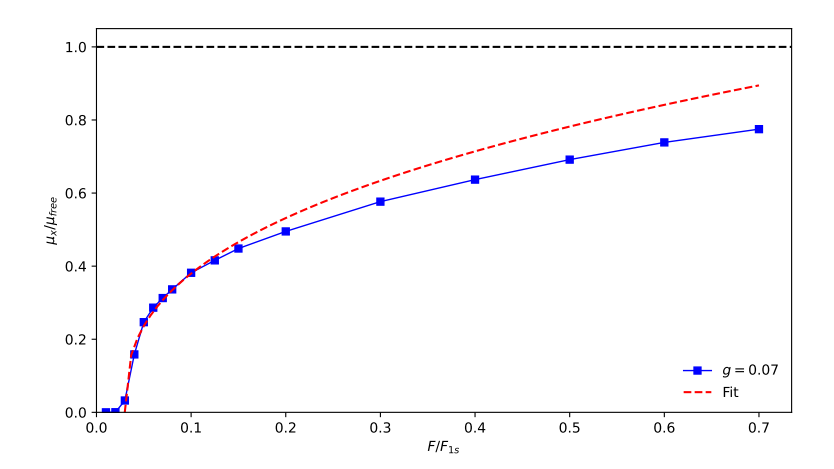


Figure 12: Power function fit performed on mobility data for unpinned states with force up to $0.3 F_{1s}$. The resulting fit parameters are $F_s = 0.1352 F_{1s}$, B = 1.2260, $\alpha = 0.5557$. The data matches the fit results for the adopted range of forces, but significantly deviates outside of that range.

window 0.01 < g < 0.04 where we can estimate that F_s vanishes.

Assessing the presence of superlubricity and the precise position and nature of the Aubry transition is a difficult task that goes beyond the computational resources available for this work. It would certainly require re-examining the problem with larger sample sizes and make a serious size scaling of the depinning thresholds.

5 Discussion and Conclusion

In this work we study the properties of an elastically deformable hexagonal lattice over a quasiperiodic potential in a mismatched configuration at the optimal misfit angle. We use a circular lattice colloid sample with harmonic colloid-colloid interactions. Via FIRE relaxation and Simulated Annealing, we construct a fully relaxed optimal starting point for successive friction simulations, verify that the results are in agreement with NM theory predictions. Simulated Annealing leads to better results than FIRE for values $g = \frac{V_0}{ka_{coll}^2} > 0.05$. larger sizes of the sample and at smaller forces, we predict that evidence of a superlubric phase may be observed. By mapping the static friction threshold as a function of the corrugation amplitude, we find evidence of an Aubry transition from a superlubric state at low corrugation to a statically pinned state in the vicinity of g = 0.05. We also find preliminary evidence of directional locking in the sliding near and

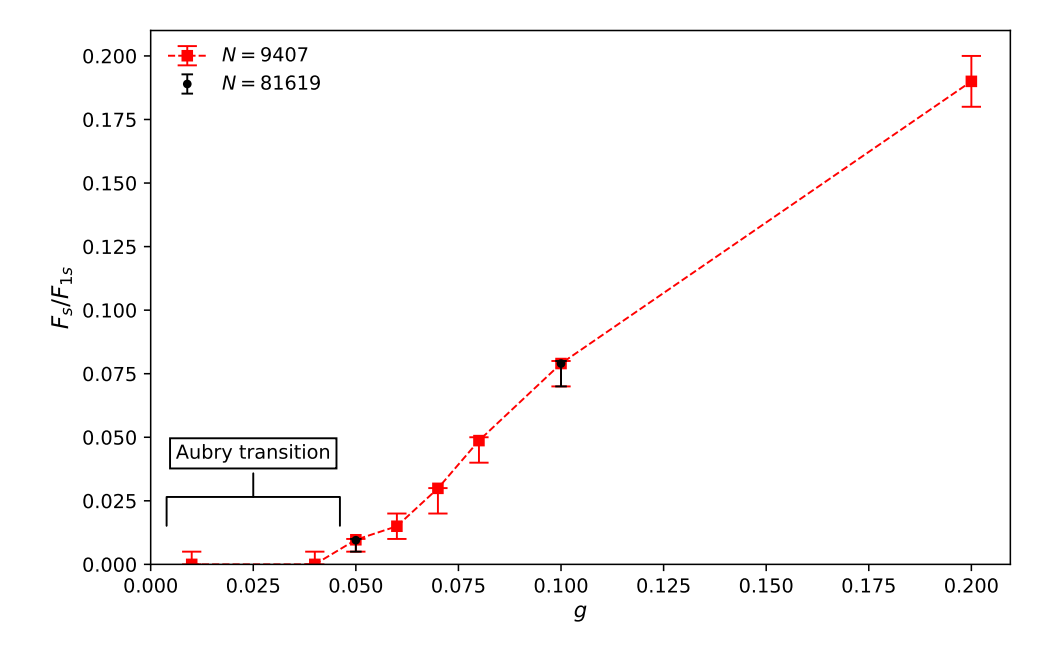


Figure 13: Confidence ranges for the depinning transition and estimated static friction threshold, Red data points are measured using a lattice sample of N=9407 particles. Black data points have been obtained using a sample of N=81619 particles. The Aubry-type transition is estimated in the 0.01 < g < 0.04 range.

above the Aubry transition.

The preliminary results obtained in this work would require a systematic size scaling to verify the presence and nature of the Aubry transition in this unconventional 2D model. Also, it would be interesting to examine the possible anisotropies of friction as a function of the driving direction.

References

- [1] O. M. Braun and Y. S. Kivshar, *The Frenkel-Kontorova Model: Concepts, Methods, and Applications*, Springer, New York (2004).
- [2] L. M. Floría and J. J. Mazo, Dissipative dynamics of the Frenkel-Kontorova model, Adv. in Phys., 45(6):505–598 (1996).
- [3] S. Aubry and P.Y. Le Daeron, The discrete Frenkel-Kontorova model and its extensions: I. Exact results for the ground-states, Phys. D, 8(3):381–422 (1983).
- [4] M. Peyrard and S. Aubry, Critical behaviour at the transition by breaking of analyticity in the discrete Frenkel-Kontorova model, J. Phys. C, 16(9):1593 (1983).
- [5] A. D. Novaco and J. P. McTague, Orientational epitaxy—the orientational ordering of incommensurate structures, Phys. Rev. Lett., 38:1286–1289 (1977).
- [6] J. P. McTague and A. D. Novaco, Substrate-induced strain and orientational ordering in adsorbed monolayers, Phys. Rev. B, 19:5299–5306 (1979).
- [7] C. G. Shaw, S. C. Fain, and M. D. Chinn, Observation of Orientational Ordering of Incommensurate Argon Monolayers on Graphite, Phys. Rev. Lett. 41, 955 (1978).
- [8] T. Brazda, A. Silva, N. Manini, A. Vanossi, R. Guerra, E. Tosatti, and C. Bechinger, Experimental Observation of the Aubry Transition in Two-Dimensional Colloidal Monolayers, Phys. Rev. X 8, 011050 (2018).
- [9] D. Bertazioli, Structure, Energetics, and Dynamic Properties of a Colloidal Monolayer on a Quasiperiodic Potential Substrate, University of Milan, 2018, http://materia.fisica.unimi.it/manini/theses/bertazioli.pdf.
- [10] T. Salvalaggio, Angular analysis of a model colloidal monolayer on a quasicrystalline substrate, University Milan, 2019, http://materia.fisica.unimi.it/manini/theses/salvalaggio.pdf.
- [11] M. Forzanini, Accurate relaxation of a 2D crystal interacting with a quasicrystalline potential, University Milan, 2023, http://materia.fisica.unimi.it/manini/theses/forzanini.pdf
- [12] S. Pagano, Angular Energetics and Friction of a Harmonic Hexagonal Monolayer over a Quasicrystalline Substrate, University Milan, 2022, http://materia.fisica.unimi.it/manini/theses/paganoMag.pdf

- [13] N. Manini, M. Forzanini, S. Pagano, M. Bellagente, M. Colombo, D. Bertazioli, T. Salvalaggio, A. Vanossi, D. Vanossi, E. Panizon, E. Tosatti and G. E. Santoro, *Striped twisted state in the orientational epitaxy on quasicrystals*, Phys. Rev. Lett. 134, 066202 (2025).
- [14] A. P. Thompson, H. M. Aktulga, R. Berger, D. S. Bolintineanu, W. M. Brown, P. S. Crozier, P. J. in 't Veld, A. Kohlmeyer, S. G. Moore, T. D. Nguyen, R. Shan, M. J. Stevens, J. Tranchida, C. Trott, S. J. Plimpton, LAMMPS a flexible simulation tool for particle-based materials modeling at the atomic, meso, and continuum scales, Comp Phys Comm, 271, 10817 (2022).
- [15] E. Bitzek, P. Koskinen, F. Gahler, M. Moseler, and Peter Gumbsch, *Structural Relaxation Made Simple*, Phys. Rev. Lett. 97, 170201 (2006)